1.16 ANNUAL VARIABILITY OF HEAT IN THE ARCTIC MIXED LAYER BENEATH PACK ICE FROM DRIFTING BUOY OBSERVATIONS

Richard A. Krishfield *

Woods Hole Oceanographic Institution, Woods Hole, Massachusetts

ABSTRACT

In order to obtain a better understanding of the large-scale structure and temporal variability of the oceanic heat flux (*Fw*) from the ocean to the ice in the Arctic, observations of heat in the mixed layer and ice dynamics are compared with parameterizations and climatologies. Long term drifting platform observations of temperature and salinity between 8 and 12 m (primarily from SALARGOS and IOEB buoys) are used to describe the annual cycle of temperature above freezing (*Taf*) in the mixed layer beneath Arctic pack ice between 1975 and 1998, and *Fw* is estimated by modulating the observed *Taf*s with ice-ocean friction velocities (*u**) determined from the platform drifts, according to the McPhee (1992) relationship. In the Transpolar Drift, *Taf* is not negligible in winter, which implies a positive *Fw* to the ice pack by means other than solar heating. In the Beaufort Gyre, variability of *Taf* (and *Fw*) between different years is apparent and sometimes not negligible in winter. A parameterization based solely on the solar zenith angle (with a 1 month lag) is found to largely describe the observed *Taf*s (with root-mean-square error less than 0.05 °C), despite the lack of an open water term. Correlations between the observed annual *Taf*s and the parameterization are high (median R^2 = 0.75), compared to *Taf*s determined from a hydrographic dataset based on the US-Russian EWG Atlas (median R^2 = 0.16). Deviations of observed *Taf*s from the parameterization cannot consistently be explained by local open water fraction anomalies (determined from satellite ice concentration data), but are likely due to heat advected horizontally, or entrained from below the halocline (such as from synoptic storms). A monthly *Fw* "climatology" from 1979 to 1998 is produced by modulating parameterized *Taf*s with *u** based on monthly ice drift averages from the IABP, also using the McPhee (1992) equations. Correlations are moderate between the derived climatology and *Fw* estimates from the drifting observations (median R^2 = 0.45), with deviations predominantly due to errors associated with *u** which are enhanced by the nonlinearity of the heat flux relationship. In the derived climatology, the interannual variations in *Taf* are fixed by the parameterization, but the dynamics cause an overall positive trend in average Arctic *Fw* since 1981.

1. Introduction

The oceanic heat flux (*Fw*) of the Arctic Ocean, the product of heat and turbulence at the ice-ocean interface, is a sensitive but poorly understood component of recent global climate change studies. Most of the heat that is transmitted to the underside of the ice pack is suspected to be from solar radiation rather than from upwelling warmer water (Maykut, 1982). Typical estimates for the central Arctic are 4 W m^{-2} from June through August and 0 W m^{-2} for the remainder of the year (Moritz et al., 1993). Although models indicate that the equilibrium mean thickness of the Arctic ice pack is sensitive to small changes in the annual average oceanic heat flux (Maykut and Untersteiner, 1971), lack of direct observations has prevented greater resolution. Discerning the seasonality of the heat and salt budgets between the ice pack and upper ocean, and the significance of transient effects on these balances, are important concerns for understanding changing Arctic sea ice mass balance and upper ocean variability.

* Corresponding author address: Richard A. Krishfield, Woods Hole Oceanographic Institution, Dept. of Geology and Geophysics, Clark 128, MS 23, Woods Hole, MA 02543-1541; e-mail: rkrishfield@whoi.edu

Direct turbulence measurements require frequent, high precision determinations of temperature, salinity, and vertical velocity in the near-surface boundary layer under drifting sea-ice (e.g. McPhee and Stanton, 1996). The turbulent fluxes are computed using a Reynolds analogy to estimate ensemble mean deviations from the covariances. Based on direct measurements from 3 ice camps, a simplified parameterization (McPhee, 1992) has been developed to estimate *Fw* by modulating the mixed layer temperature above freezing (*Taf*) by the ice-ocean friction velocity (*u**), where *u** is determined from a statistical relationship based on ice drift velocity.

In this investigation, observations of heat in the Arctic mixed layer and ice dynamics are compared with parameterizations and climatologies in order to obtain a better understanding of the large-scale structure and temporal variability of *Fw*.

2. Data

2.1. Observations

The primary hydrographic data analyzed here are time series of measurements at 8 or 10 m depths from 21 SALARGOS buoys and 2 Ice-Ocean Environmental Buoys (IOEBs) that were deployed between 1985 and 1998 at various locations across the Arctic. Usually

between 1 and 5 buoys were deployed at any time. These are augmented with historical STD or CTD data from the AIDJEX, FRAM, CEAREX, and SHEBA ice camps (Table 1). Since all of these platforms are fixed to the floating icepack, ice drift vectors may be computed from location timeseries (Figure 1). The drift pattern of ice floes (and buoys) generally fall into two categories: west (Canada basins) or east (Eurasian basins) Arctic. The west is characterized by the Beaufort Gyre surface cyclonic circulation and near surface salinity minimum, while the east is characterized by the surface Transpolar Drift that exports sea-ice through the Fram Strait. In the Transpolar Drift, high heat fluxes from entering Atlantic Water have been documented at synoptic scales (Steele and Morison, 1993).

TABLE 1. Duration and dates of observations.

Platform	obs*	start	day	end	day
Beaufort Gyre time series					
AIDJ_BB	211	Apr-75	(102)	Oct-75	(274)
AIDJ_BF	307	May-75	(132)	Apr-76	(112)
AIDJ_CB	408	May-75	(135)	Apr-76	(117)
AIDJ_SB	296	May-75	(138)	Apr-76	(112)
SAL_947	168	Apr-85	(106)	Oct-85	(304)
SAL_895	347	Apr-86	(94)	May-87	(121)
SAL_896	101	Sep-86	(268)	Jan-87	(28)
SAL_897	238	Sep-86	(257)	Jul-87	(182)
SAL_289	206	May-88	(131)	Nov-88	(335)
SAL_369	39	Mar-90	(83)	Apr-90	(120)
SAL_790	381	Apr-92	(107)	Apr-93	(120)
SAL_797	120	Sep-93	(247)	Dec-93	(365)
SAL_795	129	Oct-93	(297)	Mar-94	(60)
B96IOEB	338	May-96	(122)	Apr-97	(98)
B97IOEB	264	Apr-97	(102)	Dec-97	(365)
SHEBA	327	Oct-97	(291)	Sep-98	(273)
Total	3880				
Transpolar Drift time series					
FRAM_1	87	Mar-79	(90)	May-79	(126)
SAL_283	245	May-88	(123)	Dec-88	(366)
SAL_285	280	May-88	(147)	Feb-89	(59)
SAL_288	828	May-88	(143)	Aug-90	(213)
SAL_286	30	Jun-88	(154)	Jul-88	(183)
CEAREX	80	Oct-88	(297)	Dec-88	(366)
CEAREXO	29	Mar-89	(89)	Apr-89	(118)
SAL_284	685	Apr-90	(107)	Feb-92	(60)
SAL_103	396	Sep-90	(270)	Nov-91	(299)
SAL_104	342	Sep-90	(268)	Aug-91	(243)
SAL_108	39	Sep-90	(267)	Oct-90	(304)
SAL_792	48	Mar-91	(74)	Apr-91	(120)
SAL_793	46	Apr-92	(108)	May-92	(152)
SAL_794	199	Apr-92	(108)	Oct-92	(305)
SAL_798	181	Sep-93	(245)	Feb-94	(59)
T94IOEB	107	Apr-94	(103)	Jul-94	(210)
SAL_798	159	May-94	(147)	Nov-94	(305)
Total	3781				

* daily (buoy) or semi-daily (ice camp) averages.

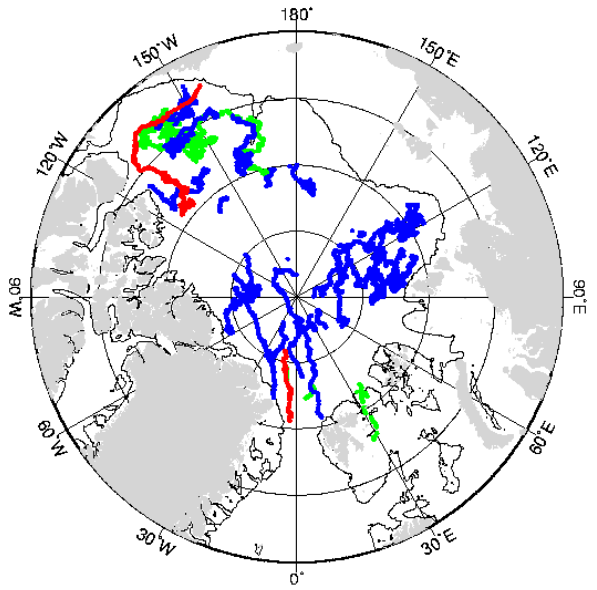

FIGURE 1. Drift tracks of SALARGOS (blue) and IOEB (red) buoys and ice camps (green). The solid line indicates the 300 m bathymetric contour.

SALARGOS (or Polar Ocean Profiler) buoys are ice-tethered drifters with Argos location, air temperature and pressure, and six SeaBird temperature and conductivity sensor pairs suspended beneath the ice to as much as 300m (Morison et al., 1982). Here the data utilized is from the uppermost seawater measurement at 10 m, which is usually located in the surface mixed layer below local surface disturbances. Twenty-four SALARGOS buoys were deployed throughout the Arctic between 1985 and 1996 by the Polar Science Center, University of Washington. The lifetime of the expendable systems varied from as little as 1 month to over 2 years. These data were contributed to the Joint Russian-American Environmental Working Group Arctic Atlas CD-ROMs (EWG, http://www-nsidc.colorado.edu/data/ewg/), and are provided on the International Arctic Buoy Program (IABP; http://iabp.apl.washington.edu) CD-ROM (Version 1.0) in 12 minute and 10 day averages. The accuracy of the SeaBird sensors are expected to be about ±0.01° C and ±0.05 PSU, but without post-deployment calibrations, it is impossible to precisely determine sensor drifts. However, obvious malfunctions and a few spurious Argos locations were removed, resulting in 5207 days of temperature and salinity observations at 10 m from 21 SALARGOS buoys.

The IOEB system consists of a surface flotation package which supports the meteorological and ice sensors, and houses data loggers, transmitters, antennae, and batteries (Krishfield et al., 1993; Honjo et al., 1995; Krishfield et al., 1999). Suspended from the surface float is a 110 m long mooring system that includes precision salinity and temperature recorders, current profiling, and biogeochemical sensors. In April 1996, an IOEB in the Beaufort Gyre was recovered after

4 years of drift since being deployed at the LEADEX ice camp. Sensors and batteries were replaced, and the system was redeployed on a similar nearby icefloe within one week. In April 1997, the system was again visited, and sensors and batteries were replaced. Although this IOEB was subsequently never recovered, over 2 years of near-continuous data from the air, ice, and upper sensors were made available via Argos satellite transmission. Another IOEB was deployed north of Fram Strait in the Transpolar Drift, and drifted for 9 months before being recovered east of Greenland.

SeaBird SBE-16 SeaCats are used at three locations (8, 43 and 75 m) along the IOEB mooring for salinity and temperature measurements. Data from the instrument at 8 m on both of IOEBs described above are presented. The temperature measurements are accurate to ±0.01° C and the salinity to ±0.05 PSU, although modest uncertainties exist in the depth determinations due to mooring declination. Calibrations were performed before being deployed in 1996 and in 1997, and indicate that sensor drifts for the moored instruments are within the stated accuracies (temperature <0.005 C yr^{-1}, salinity <0.002 $month^{-1}$). Because the IOEB redeployed in 1997 was not recovered, no post calibration of the 1997-98 SeaCat data were performed. However, there were no obvious errors indicated in the data that were telemetered.

Although ice camp hydrographic measurements have historically been acquired less frequently than these buoy data, they do provide additional timeseries of mixed layer properties and ice drift, and sometimes other independent heat flux observations. Semi-daily STD data from the four AIDJEX ice camps in the Beaufort Sea were obtained from the National Snow & Ice Data Center (NSIDC; http://www-nsidc.colorado.edu/), spanning the period April 1975 to April 1976 (Bauer, 1980; Maykut and McPhee, 1995). Also available from the NSIDC, the CEAREX CD-ROM provides CTD data in the Transpolar Drift from CEAREX in autumn 1988 and the CEAREX oceanography camp in spring 1989, as well as STD data from the spring Fram 1979 and 1981 ice camps. From October 1997 to September 1998, the SHEBA ice camp employed a yo-yo CTD down to 150 m depth (Stanton, T., D. Kadko, D. Martinson, M. McPhee, J. Morison, L. Timokhov: Upper Ocean Structure and Regional Heat Content Measured During SHEBA, *J. Geophys. Res.*, to be submitted), and this data was obtained from the CODIAC website via the SHEBA homepage (http:// sheba.apl.washington.edu/).

2.2. Climatological data

For comparison with the observations, and to provide similar information on broader temporal and spatial scales across the entire Arctic basin, a hydrographic climatology and ice drift dataset are employed.

Mean monthly temperature and salinity information at 1° grid spacing and standard depths were obtained from the Polar Hydrographic Climatology (PHC; Steele et al., 2001). The PHC is a merged dataset combining the accuracy but low temporal resolution of the EWG at high latitudes (only two climatological seasons) with the relatively data poor (without the historical Russian data), but higher temporal resolution of the World Ocean Atlas (WOA; http://www.nodc.noaa.gov/). However, 1) the annual cycle is derived from winter and summer endpoints by applying an arbitrary cyclic function, and 2) there is a seam between 82.5 and 83 °N. For the purposes of this study, the mixed layer properties are characterized by the temperature and salinity values at 10 m. Since the PHC climatology is described for only one annual cycle, interannual or decadal variations in thermal and freshwater budgets are neglected.

Monthly grids of ice drift vectors from 1979 through 1998 were obtained from the IABP CD-ROM. Locations from a variable array of surface drifters provides the raw data that is optimally interpolated onto a 100 km Polar stereographic grid.

3. Methods

Using the mixed layer temperature and salinity, and ice drift data previously described, the quantities that are evaluated are: sigma (σ), *Taf*, u^*, and *Fw*.

The freezing points of seawater and σ are calculated from the seawater temperature, salinity, and pressure (converted from depth) using the CSIRO toolkit (ftp://ftp.marine.csiro.au/pub/morgan/seawater/) based on UNESCO 1983 equations (Fofonoff and Millard, 1983). *Taf* is merely the difference of the temperature from the freezing point temperature. Either adding heat or removing fresh water will elevate *Taf* in seawater of fixed pressure and volume.

A statistical relationship (McPhee, 1979) is used to determine u^* from the square root of the kinematic ice-ocean stress (τ), where:

$$\tau = 0.0104 * V^{1.78} \quad (1)$$

and V is the difference of the ice velocity from the surface geostrophic current velocity.

Inherent in the relationship are Rossby similarity constants, and the undersurface roughness (z_0), which were fixed based on AIDJEX measurements. Recent results from the SHEBA ice camp (McPhee, 2002) suggest that z_0 for undeformed multiyear ice is an order of magnitude less than the AIDJEX estimates, which would reduce the calculated u^* considerably. Therefore, there is an undetermined amount of error associated with specifying z_0. Furthermore, because the geostrophic current in the Arctic is relatively small (typically less than 5 cm/s, with the exception of local submesocale eddies in the halocline), it is neglected here when evaluating τ, and this is another potential source of error.

Using the McPhee (1992) parameterization, *Fw* is estimated by modulating the mixed layer *Taf* by u^* according to the equation:

$$Fw = \rho\, c_p\, c_h\, u^*\, Taf \quad (2)$$

where ρ is seawater density (= 1000 + σ), c_p is specific heat of seawater near freezing (= 3980 J kg^{-1}), and c_h is the heat transfer coefficient (= 0.006).

4. Results

4.1. σ, Taf, and u from observations*

The hydrographic data from the platforms listed in Table 1 are used to calculate seawater σ and *Taf* from each measurement from the instrument located at either 8 or 10 m in the case of buoys, or from averages between 8 and 12 m in the case of STD or CTD profiles. The values determined from the higher resolution buoy data and SHEBA yo-yo CTD are subsequently averaged on a daily basis, while the semi-daily profiles from the other ice camps are not averaged. Ice drift velocities are calculated from the raw locations, and *u** is determined from each velocity and subsequently averaged in the same increments as the density and *Taf*. Consequently, a total of 7661 points result from the observations.

In Figures 2, 3, and 4 all of the computed daily or semi-daily values of σ, *Taf*, and *u** from all platforms are plotted versus day of the year. Even in this coarse representation, some broad features of the time series stand out.

There are significant geographical variations in the density data (the surface waters in the Canada Basins are fresher), but an annual cycle is also apparent. In general, the density appears to decrease moderately from May (~day 150) to November (~day 300), and increases otherwise. As the temperature is close to freezing, σ is controlled mostly by the salinity, so the changes in σ mostly reflect the annual cycle of growth and ablation of the overlying sea ice.

There is a clear annual cycle in the *Taf* data, which increases in May, attains a peak around the end of July (~day 210) and decreases rapidly thereafter, and appears to vary relatively uniformly throughout the Arctic basins. Between November and May, *Taf* is generally less than 0.03°C, except for a few instances. In particular, the enhanced Tafs evident around day 300 are from IOEB data, and these have been attributed to the entrainment of warmer sub-halocline water due to the passage of synoptic storms (Yang et al., 2001).

On the other hand, there is some suggestion of an annual trend in the *u** data during the summer months, but the signal in the winter months is not clear. As indicated previously, the calculations of *u** from ice velocity depend on the roughness of the sea ice and the upper ocean geostrophic velocity, and neglecting variations of these terms could be responsible for some of the uncertainty. Furthermore, the parameterization assumes that the ice is freely drifting without internal ice stresses, which may not always be the case, especially in the winter months. Overall, there is a much larger amount of synoptic variability in *u**, than in either density or *Taf*. In monthly average data, this short-term variability cannot be precisely expressed, so becomes another source of error when *Fw* is estimated using climatological ice velocities.

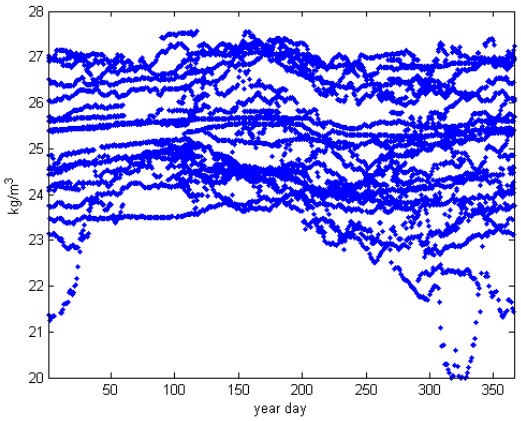

FIGURE 2. Daily or semi-daily averages of σ as a function of year day from observations.

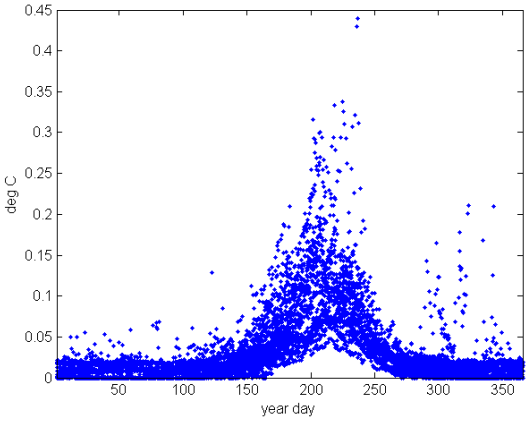

FIGURE 3. Daily or semi-daily averages of *Taf* as a function of year day from observations.

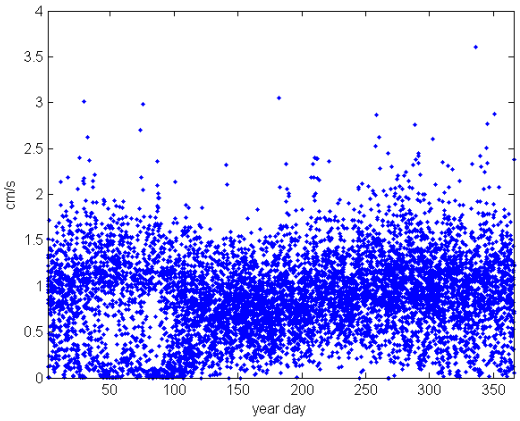

FIGURE 4. Daily or semi-daily averages of *u** as a function of year day from observations.

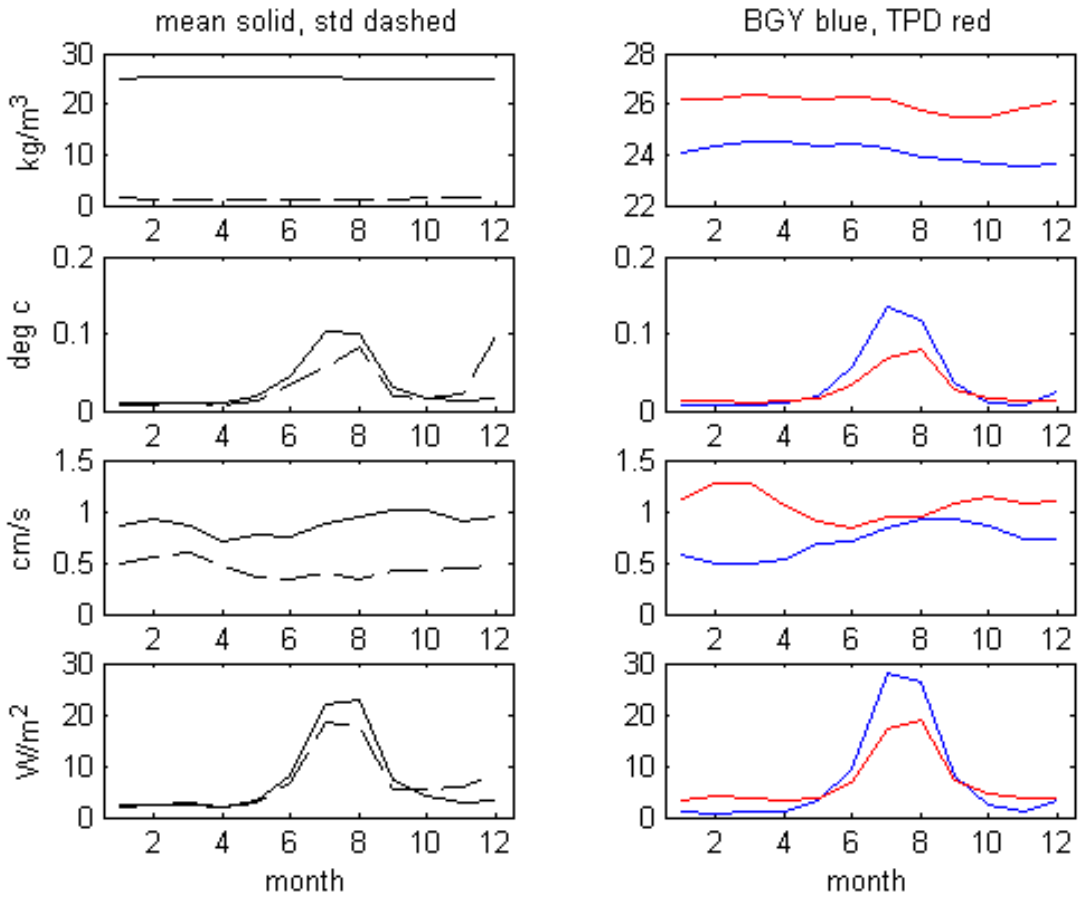

FIGURE 5. Left panels: monthly means (solid lines) and standard deviations (dashed lines) of σ, *Taf*, u^*, and *Fw* from all platforms. Right panels: monthly means from platforms in the Beaufort Gyre (blue) and Transpolar Drift (red).

4.2. Annual variability from observations

Monthly statistics of the quantities determined from observations are calculated altogether, and separately from the platfoms in the Transpolar Drift and Beaufort Gyre regions (Figure 5). On an annual basis, mean annual *Fw* in the Beaufort Gyre (7 W m^{-2}) is marginally greater than in the Transpolar Drift (6 W m^{-2}).

A large part of annual variability can be related to a latitudinal dependence on the solar insolation. In the summer, the heat in the upper ocean and flux of heat are larger in the Beaufort Gyre than the Transpolar Drift. *Fw* is not negligible in winter, but is reduced to less than 2 W m^{-2} in the Beaufort Gyre, and is approximately 3 W m^{-2} in the Transpolar Drift.

4.3. Taf Parameterization

Taf is the most significant component of the annual cycle of *Fw*, and σ is the least. For comparison with the observations from the drifting platforms, a climatological *Taf* is also calculated from values of temperature and salinity at 10 m depth from the PHC. A scatter plot of *Taf* from observations versus *Taf* from the climatology is presented in the upper left panel of Figure 6. For the most part, *Taf* from the climatology overestimates *Taf* from the observations, and the standard deviation of the difference is 0.2°C. Consequently, correlations between each time series from the drifting platforms and the corresponding climatological values are low (median R^2 = 0.16).

A relatively simple statistical relationship based on the solar zenith angle (α) reproduces the observed annual signal of *Taf* with less error than the climatology. Out of all 33 time series from observations, only 17 which spanned most of the annual cycle were selected for parameterizing *Taf*. Using a least squares fitting algorithm the following relationship was determined:

$$Taf = 3\cos(\alpha(t - 33))^6 + 0.01 \qquad (3)$$

Where α is determined from the latitude and time, including a 33 day time lag. A contour plot of the parameterized values of *Taf* by day of year and latitude is presented in Figure 7. The offset that is added at the end of the equation often overestimates the observed *Taf* in winter in the Beaufort Gyre, but underestimates *Taf* in winter in the Transpolar Drift.

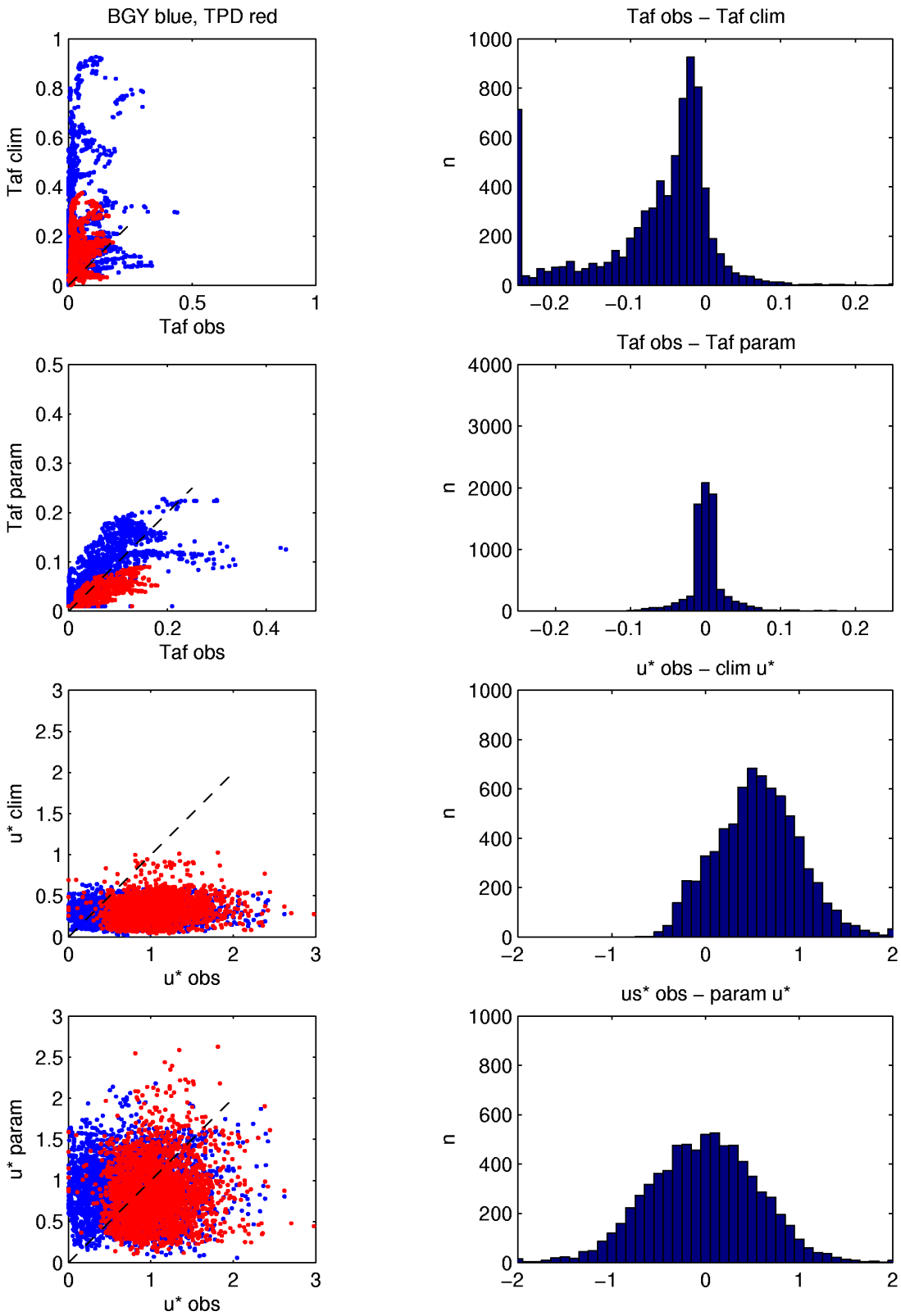

FIGURE 6. Left panels: scatter plots of *Taf* and *u** from observations versus the corresponding values from climatologies and parameterizations. Data from the Beaufort Gyre is blue and Transpolar Drift is red. Right panels: histograms of differences between *Taf* and *u** from observations, and climatologies and parameterizations.

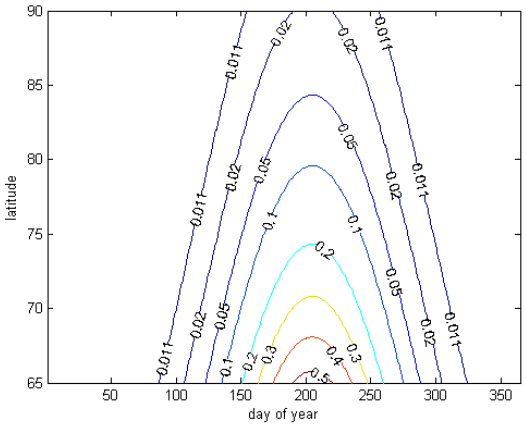

FIGURE 7. Parameterized *Taf* (°C) as a function of α, year day and latitude.

As can be seen from the second row of panels in Figure 6, the parameterized *Tafs* are a better fit to the *Tafs* from observations, such that the standard deviation of the differences is less than 0.05°C. Furthermore, correlations between time series of *Taf* from the observations and time series reconstructed from the parameterization are correspondingly high (median R^2 = 0.75).

4.4. Fw "climatology"

The parameterized *Taf* are modulated with mean monthly ice drift vectors for the years 1979 through 1999 from the IABP. However, σ is estimated from the PHC climatology with sufficient accuracy to have only a negligible effect on *Fw*. Similar to the time series calculations, the geostrophic flow is not removed from the ice drift.

Values of u^* computed from the ice drift climatology were consistently less than the observations (third row of panels in Figure 6). A least-squares regression determined that the difference from the observations is minimized by multiplying u^* derived from the climatology by a factor of 3 (lower panels of Figure 6).

Maps of monthly climatological heat flux maps were prepared from the 20-year dataset, and mean annual, variance, and multiyear averages were determined, based on cyclonic (1980-1983 and 1989-96) and anticyclonic (1984-1988 and 1997-1998) circulation regimes (Proshutinsky and Johnson, 1997). The mean and standard deviation are plotted in the top panels of Figure 8, while mean anomalies for each circulation regime are plotted in the bottom panels.

Due to the relationship of *Taf* with α, the variability in *Fw* increases significantly from less than 1 W m^{-2} at the North Pole to more than 10 W m^{-2} south of 80°N. On the other hand, the minimum in annual average *Taf* is displaced from the North Pole toward the Canadian Archipelago (near 85°N, 90°W). Throughout the Arctic, *Fw* is marginally elevated (0.5 to 1 W m^{-2}) during the cyclonic circulation regimes, versus reduced by about the same magnitude during the anticyclonic circulation regimes. Coincidentally, there are significant anomalies of *Fw* in the opposite sense in the Canada Basin. Correlations of *Fw* from the parameterized "climatology" with *Fw* derived from observations are moderate (median R^2 = 0.45).

5. Discussion

The observations provide time series of heat and velocity at various locations through the Arctic Ocean, while the parameterized "climatology" fixes the annual cycle of heat to the solar angle, and varies u^* according to an optimally interpolated atlas of ice velocities. Temporal and regional averages from observations provide the most precise information, but represent only

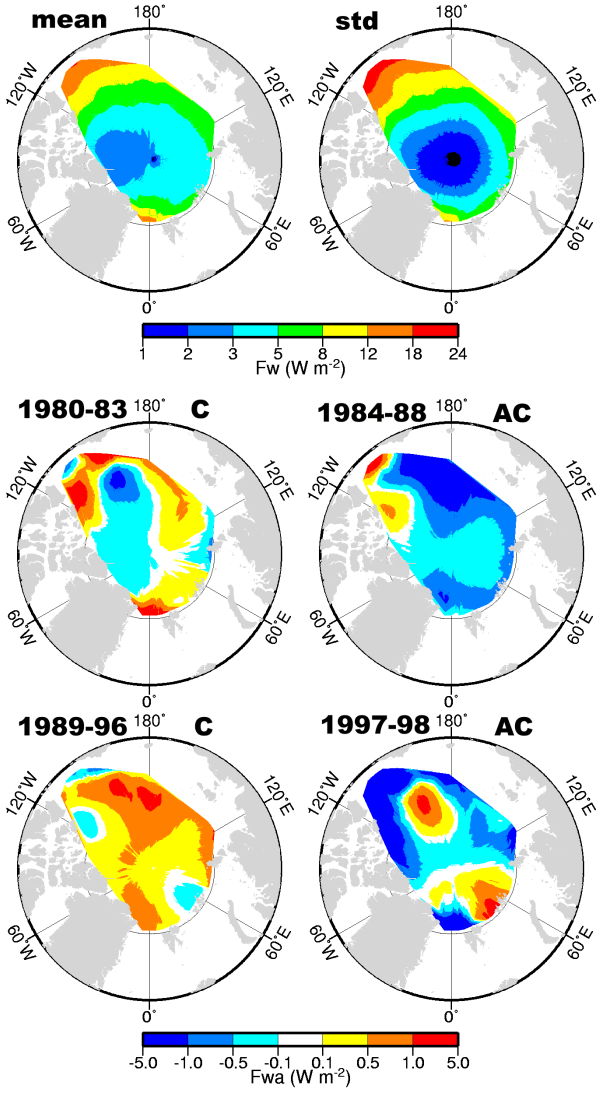

FIGURE 8. Annual means and standard deviations of *Fw* (W m^{-2}), and anomalies from mean during cyclonic (left) and anticyclonic (right) circulation regimes using parameterized *Taf* estimates and u^* from monthly IABP ice drifts.

certain times and locations. The "climatology" expands the geographic extent and frequency of the data, but varies only due to the turbulent component. The residual difference between the observations and the "climatology" are the time varying thermodynamic changes. By combining the estimates from both datasets, some characteristics of the spatial structure and temporal variability of *Fw* to the Arctic pack ice are discerned.

Specifically, annual estimates of the magnitude of *Fw* for different regions and times are computed from the observations and the "climatology." Because the distribution of the observations in space-time is large, the parameterized "climatology" is used to determine how well these estimates represent the whole Arctic Ocean. The magnitudes determined from the observations are used to adjust *Fw* averages from the parameterization, to produce first order space-time *Fw* estimates. The time varying components of *Fw* are divided into heat (*Taf*) and turbulent components (*u**). The variations in the heat are further subdivided into components due to the annual cycle (parameterized *Taf*), and those due to interannual variability (residuals). Quantities are tabulated for each component, and based on barotropic circulation regimes to enumerate the relative contribution of each to the total *Fw* budget, and how each component varies. Finally, the *Fw* trend due to the turbulent component is described.

5.1. Annual estimates of Fw

The high correlation of the parameterized *Taf* to the observations suggests that the angle of the solar incidence is the primary source of the heat in the mixed layer beneath the pack ice. The observations were all obtained where mean annual ice concentrations were greater than 90%, so the results are not applied outside of the central pack. Furthermore, it is assumed that these results are representative to the basins, away from shelf processes and boundary currents. Consequently, the broad Eurasian shelf seas are not included in the study region, but there is a region in the southern Beaufort Gyre. In the more southerly region of the Beaufort Gyre, it is expected that *Fw* will be greater.

To begin with, in a previous study Maykut and McPhee (1995) used the same methods on the daily CTD data study to estimate *Fw* at the 5 AIDJEX camps in the Beaufort Sea in 1975-76. They found maximum *Fw* values reached 40 to 60 W m^{-2} in August, for an annual average value of 5.1 W m^{-2} (where they assumed zero heat flux in winter). This compares with the calculations in the present study, where annual average *Fw* at AIDJEX varies depending on ice camp from 4 to 9 W m^{-2} (and no zero assumption). However, the differences using the *Taf* parameterization are 2 to 5 W m^{-2} greater than the observations.

In fact, annual *Fw* is 9 W m^{-2} from all 10 platforms with observations through the summer in the Beaufort Gyre (Table 2). The maximum *Fw* was 19 W m^{-2} from two SALARGOS buoys in 1985 and 1988. Minimum annual *Fw* (2 W m^{-2}) was detected by the IOEB in 1996. Annual average *Taf* from the observations varied from 0.03 to 0.08 °C, and sometimes exceeded the parameterized *Taf* even in winter, but mostly the parameterization was about 0.01°C higher. The data from the SHEBA ice camp are a good example of the annual cycle. *Fw* averaged 9 W m^{-2}, although observations were elevated in summer (above parameterized *Taf*). For comparison, Perovich and Elder (2002) report annual average *Fw* at SHEBA from ice temperature profiles from four different ice types, ranging from 7.5 W m^{-2} for multiyear ice to 12.4 W m^{-2} for an old ridge.

On the other hand, in the Transpolar Drift the locations of the platforms are farther north than in the Beaufort Gyre. However, as platforms approach Fram strait, *Fw* increases considerably (e.g. Perovich et al., 1989). Overall, annual average *Fw* calculated from the 7 SALARGOS buoys deployed in the Transpolar Drift region between 1988 and 1992 is 7 W m^{-2}. The parameterized Tafs from the Transpolar platforms are mostly less than the observed Tafs by 0.01-0.02°C, and the variability between platforms is less. The elevation of heat above freezing even in winter is probably due to advection of heat horizontally or vertically from the subsurface Atlantic layer.

Averaging *Fw* from all observations equals 7 W m^{-2} (Table 2). For comparison, annual *Fw* is approximately the same from the parameterized "climatology" (Table 3). In the "climatology," *Fw* in the Transpolar Drift are biased negatively from the observations by about 2-3 W m^{-2}, which can be attributed primarily to elevated *Taf* in winter.

TABLE 2. Annual *Fw* from observations.

Year*	BGY	TPD	ALL
ALL mean	9.1	7.2	6.8
ALL std	5.8	2.6	5.0
1975-76 (AC)	6.3		
1984-88 (AC)	15.4	8.4	
1989-96 (C)	3.9	6.4	
1997-98 (AC)	9.0		

* (AC) anticyclonic and (C) cyclonic circulation regimes from Proshutinsky and Johnson (1997).

TABLE 3. Annual *Fw* from "climatology."

Years	BGY	TPD	ALL
ALL mean	9.6	3.1	6.5
ALL std	8.2	0.8	11.2
1980-83 (C)	9.5	3.0	6.7
1984-88 (AC)	9.1	2.7	6.1
1989-96 (C)	10.0	3.5	6.8
1997-98 (AC)	14.5	3.0	8.6

BGY sector is between 180-60°W and south of 85°N
TPD sector is between 60°W -180 and north of 85°N

5.2. Multiannual and Interannual variability

Multiyear averages are based on the timing of the circulation regimes of Proshutinsky and Johnson (1997). Changes in the Arctic vortex, surface pressure and winds influence the distribution of ice cover, and are presumably related to changes in the Arctic Oscillation or North Atlantic Oscillation. Alternately, fresh water is believed to accumulate and be released in the Beaufort Gyre, which may affect ice export into the Greenland Sea, and formation of the Odden ice tongue (Proshutinsky et al., 2002).

The anticyclonic circulation regime from 1984-1988 is characterized by 3 SALARGOS buoys deployed in the Beaufort Gyre and 3 SALARGOS buoys deployed in the Transpolar Drift, although data are not available for all years. The cyclonic circulation regime from 1989-1996 is observed by one SALARGOS and one IOEB time series in the Beaufort Gyre, and 4 SALARGOS buoys in the Transpolar Drift. The subsequent anticyclonic circulation regime begins in 1997, continues through 1998, and is represented by one IOEB and the SHEBA ice camp in the Beaufort Gyre. We have no data in the Transpolar Drift during this last circulation period.

Comparison of *Fw* from observations with *Fw* from the "climatology" (Table 2 and Table 3) consistently indicates that *Fw* in the Beaufort Gyre is enhanced compared to the Transpolar Drift. Because the basins and ice pack in the Beaufort Sea extend farther south than the remainder of the Arctic, *Fw* in this region are higher, and variations in the annual means from all areas largely reflect the variations in the southern Beaufort Sea. In the Transpolar Drift, which is farther north, the magnitude and variability of annual average *Fw* is less. On the other hand, mixed results are indicated for *Fw* changes during different circulation regimes.

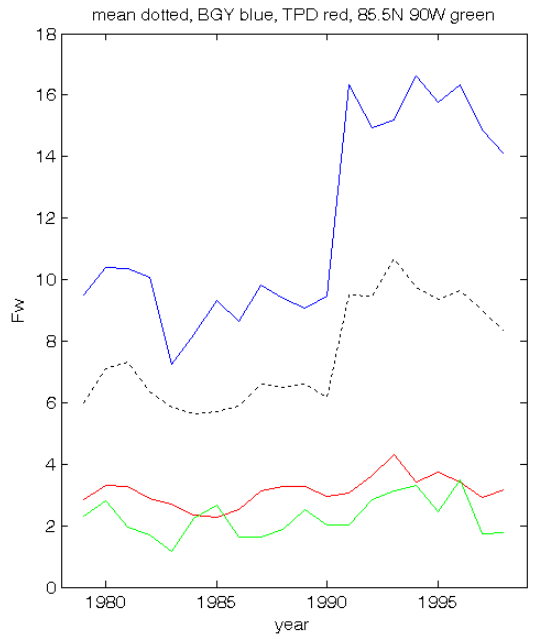

FIGURE 9. Annual average *Fw* from parameterized "climatology" in all basins (dotted), at the *Fw* minimum (green; 85°N, 90°W), in the Beaufort Sea sector (blue; between 180° and 60°W and south of 85°N) and in the Transpolar Drift sector (red; between 60°W and 180° and north of 85°N).

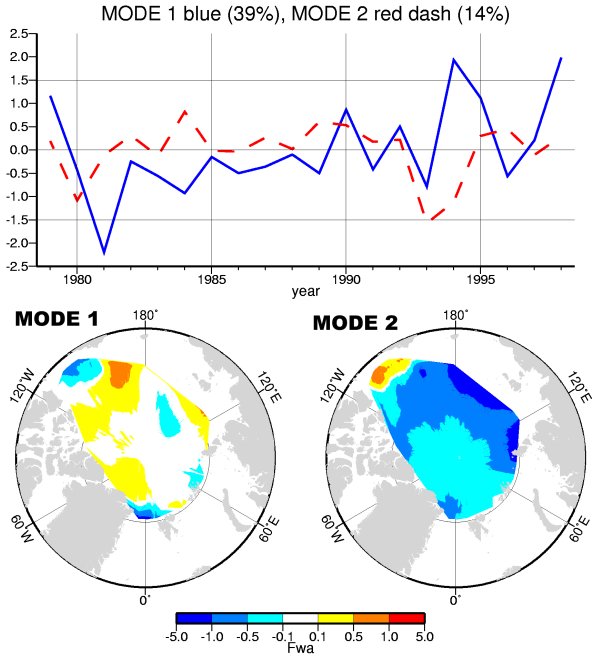

FIGURE 10. First and second EOF modes of *Fw* (W m^{-2}) variability due to *u** from monthly IABP ice drifts and using parameterized *Taf* estimates.

In Figure 9, annual averages from the parameterized "climatology" from 1979 to 1998 are presented for selected regions. The average for all areas covered by the grid is given by the black dotted line. A sector average that encompasses the Beaufort Sea is by blue, and the remaining sector average describing the Transpolar Drift is indicated by red. From Figure 8, the minimum of mean annual *Fw* from the "climatology" is located near 85°N, 90°W, and annual mean *Fw* at that location is indicated by the green line in Figure 9.

The ice-ocean friction mixes the heat, and is associated with another portion of the variability of *Fw*. Using Singular Value Decomposition (SVD) on the parameterized monthly *Fw* "climatology," the first two modes of interannual variability of *Fw* associated with the ice drift are identified. These are plotted in Figure 10, along with the time series, which shows an increase in *Fw* mode 1 since 1981, accompanying an overall increase in *Fw*, particularly in the Beaufort Gyre. This mode describes nearly 40% of the variability, and has an increasing trend over the 20-year duration of the climatological ice drift data.

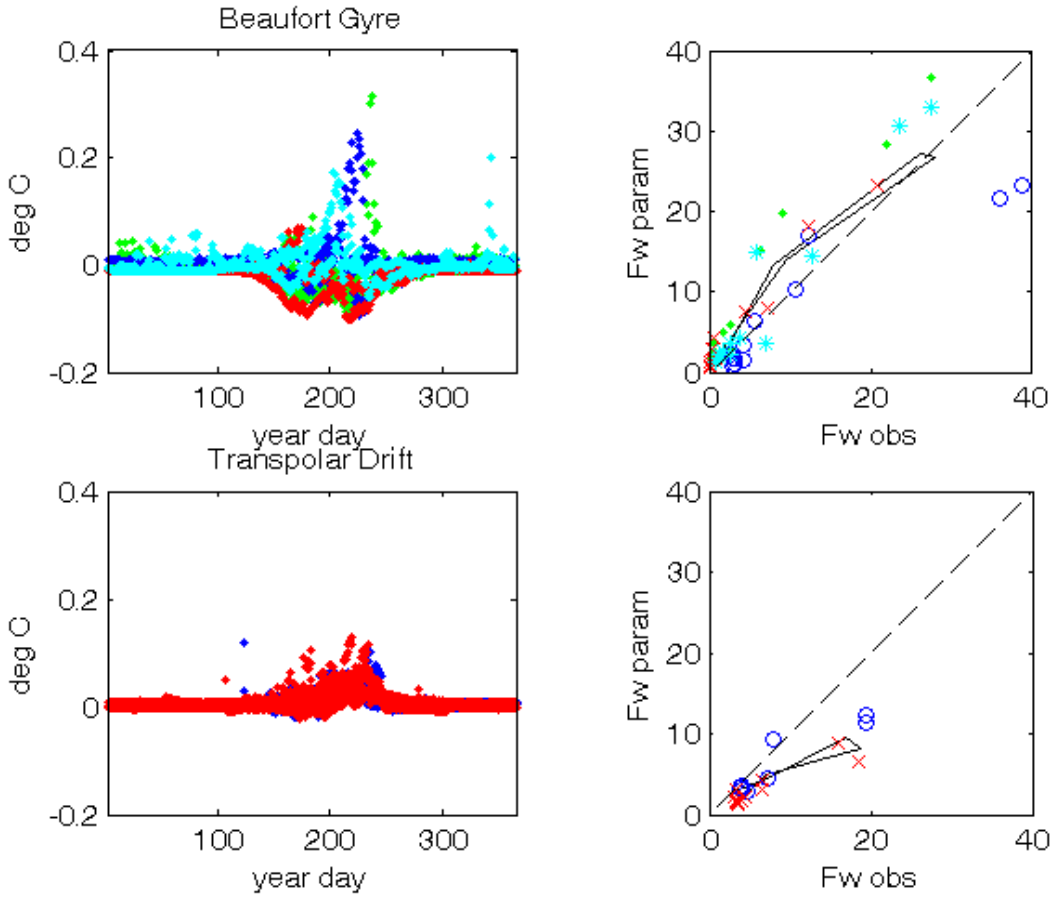

FIGURE 11. Residuals in Beaufort Gyre (top) and Transpolar Drift (bottom) during AIDJEX (green), 1984-88 (blue), 1989-97 (red), 1997-98 (cyan). Left panels: differences of *Taf* from observations with *Taf* from parameterization as a function of year day, and right panels: corresponding monthly averages of *Fw* from observations versus *Taf* parameterization. The black line is the monthly averages from all platforms in each region.

5.3. Residual analysis

The residual time series that result from the difference of the observations from the *Taf* parameterization constitute anomalies that include all other variability than the solar angle. These include all the effects of the albedo and cloud properties as well as any internal ocean variability. The residuals are plotted in Figure 11 with different colors depicting the data for different time periods corresponding to circulation regimes.

The main difference that stands out is that the heat (*Taf*) and the *Fw* from observations are always higher than the same properties as parameterized in the Transpolar Drift, but not in the Beaufort Sea. As *Fw* from observations increases to 10 W m^{-2}, *Fw* from the *Taf* parameterization is overestimated by as much as 5 W m^{-2}. Peak summer *Fw* from observations typically exceeds *Fw* from the parameterization in both oceans. Part of this signal can be attributed to error in the parameterization. On the other hand, in the winter Transpolar Drift data, there is a constant residual *Fw*, which is probably a component of heat mixed from below or advected from the perimeter.

In order to determine whether the residuals could be simply correlated to the extent of the ice pack (which has large effects on the sensible and latent transfers of heat between the ocean and atmosphere, as well as albedo), anomalies of ice concentration from satellite data were compared to the residuals, but no consistent patterns were evident. Only in some cases did a large ice concentration anomaly correspond to a large residual.

Mean annual *Fw* from the residuals are shown in Table 4. The residual *Fw* is approximately 10% of the total annual average. Adding *Fw* from the residuals (Table 4) to *Fw* from the parameterization (Table 3) distributes the residual signal from the observations over the entire Arctic and provides a basin scale estimate of *Fw*. The annual average value of *Fw* estimated this way is 8 W m^{-2} in the Beaufort Gyre, 6 W m^{-2} in the Transpolar Drift, for an average of 7 W m^{-2} throughout the Arctic.

TABLE 4. Annual *Fw* from residuals.

Year*	BGY	TPD	ALL
ALL mean	-1.5	3.2	0.7
ALL std	11.5	5.8	9.1
1975-76 (AC)	-4.3		
1984-88 (AC)	3.6	3.0	
1989-96 (C)	-2.3	3.3	
1997-98 (AC)	-2.2		

* (AC) anticyclonic and (C) cyclonic circulation regimes from Proshutinsky and Johnson (1997).

5.4. Uncertainties

Unfortunately, due to the measurement errors, a large amount of regional variability, and approximations in the parameterizations, the uncertainty in the calculations is large. Assuming that the underice roughness estimate applies to all platforms, the resolution of the *Fw* estimates are taken to be 1 W m^{-2}, while the daily values are only as precise as 5-6 W m^{-2}. Averaging monthly data brings the precison of the *Fw* estimates down to about 1 W m^{-2}.

This uncertainty is the same magnitude as the interannual variability from the parameterized "climatology" over most regions of the Arctic, except for the Beaufort Gyre where the variability is larger. It is also comparable to time averaged results that have been obtained using ice thermistor profiles from icefloes (McPhee and Untersteiner, 1982; Perovich et al., 1989; Wettlaufer, 1991; Perovich et al., 1997). However, the same ice thermistor results indicate that there is large variability in spatial scales of only 10-100m.

6. Summary and conclusions

Observations from drifting buoys indicate that there is a significant relationship of the angle of the sun (α) with *Taf* in the upper ocean under the Arctic ice pack. As a result, *Fw* from the upper ocean to the ice depends strongly on latitude. Based on a combination of observations, climatological data and parameterizations, annual *Fw* is on average less than 4 W m^{-2} north of 80°N, but within the whole Arctic basins averages 7 W m^{-2}. These estimates are more than the 2 W m^{-2} that was required in model simulations to equilibriate a perennial ice thickness of 3 m (Maykut and Untersteiner, 1971). However, they are more consistent with other recent estimates of *Fw* from observations such as in Maykut and McPhee (1995), Perovich et al. (1997), and Perovich and Elder (2002).

Maykut and McPhee (1995) suggested that most the heat of the mixed layer enters as solar radiation through leads in the ice pack rather than being diffused upward from below. Supporting a solar association, the present study indicates that most (75%) of the annual variability of *Fw* can be attributed to the solar angle, α. However, a direct relationship with the amount of leads in the icepack was not evident in ice concentration data.

Since the Beaufort Gyre is located farther south than the Transpolar Drift, higher α means an additional area wide average *Fw* of 6 W m^{-2} in the Beaufort Gyre. On the other hand, in winter, *Fw* that cannot be ascribed to α is 3 W m^{-2} in the Transpolar Drift, and is usually negligible (but not always) in the Beaufort Gyre. One explanation for the winter *Fw* is that locally intense fluxes of heat to the surface may be entrained from below by synoptic storms (Steele and Morison, 1993; Yang et al., 2001).

The Beaufort Gyre is also where the greatest interannual variability in *Fw* is located. This variability is encountered in both the observations and the parameterizations, although changes in *Fw* according to circulation regimes are not. In the parameterization, variations in ice drift velocity in the Beaufort Gyre from the 1980s to the 1990s increase *Fw* by as much as 5 W m^{-2}, coincident with the positive shift of the Arctic oscillation (Walsh et al., 1996). Increased *Fw* in the Beaufort Sea would mean increased ice melt, consistent with upper ocean freshening described by McPhee et al. (1998). In fact, in 1998, the circulation regime shifted from cyclonic to anticyclonic, and the ice cover in the west Arctic was at a minimum (Maslanik et al., 1999; Comiso et al., 2002). Several years later (in 2002), a record minimum sea ice extent was recorded throughout the entire Arctic (Serreze et al., 2002).

In the Transpolar Drift, the existence of the cold halocline is believed to isolate the Atlantic layer heat from reaching the ice pack directly. Consequently, The retreat and recovery of the halocline (Steele and Boyd, 1998; Björk et al., 2002; Boyd et al., 2002) could influence *Fw* in the Eurasian Basins, however in the present study interannual variations from either observations or parameterizations do not appear to be significant in the Transpolar Drift.

Acknowledgments: Portions of this work were prepared with funding provided by the Frontier Research Group and International Arctic Research Center. Analysis of the IOEB data was accomplished as part of the IOEB program, which was supported by the Office of Naval Research, High Latitude Program, and Japan Marine Science and Technology Center. S. Honjo, T. Takizawa, and K. Hatakeyama are acknowledged for their contributions to the IOEB data. The author also benefited from discussions with J. Yang, D. Walsh, A. Plueddemann, and A. Proshutinsky.

REFERENCES

Bauer, E. K. Hunkins, T.O. Manley, and W. Tiemann, Arctic Ice Dynamics Joint Experiment 1975-76, Physical Oceanography Data Report, Salinity, Temperature and Depth Data, vols.1-4, *Tech Rep. 8-11*, CU-8-80–CU-11-80, Lamont-Doherty Geol. Obs., Columbia Univ., Palisades, N.Y, 1980.

Björk, G., J. Söderkvist, P. Winsor, A. Nikolopoulos, and M. Steele, Return of the cold halocline layer to the Amundsen basin of the Arctic Ocean: Implications for the sea ice mass balance, *Geophys. Res. Lett.*, 29, 10.1029/2001GL014157, 2002.

Boyd, T.J., M. Steele, R.D. Muench, and J.T. Gunn, partial recovery of the Arctic Ocean halocline, *Geophys. Res. Lett.*, 29, 10.1029/2001GL014047, 2002.

Comiso, J.C., J. Yang, S. Honjo, and R. Krishfield, The detection of change in the Arctic using satellite and in situ data, submitted to *J. Geophys. Res.*, 2002.

Fofonoff, P. and Millard, R.C. Jr, Algorithms for computation of fundamental properties of seawater, UNESCO Tech. Pap. in Mar. Sci., No. 44, 53 pp., 1983.

Honjo, S., T. Takizawa, R. Krishfield, J. Kemp, K. Hatakeyama, Drifting Buoys Make Discoveries About Interactive Processes in the Arctic Ocean, *Eos Trans. AGU, 76*, 209, 215, 1995.

Krishfield, R., Doherty, K., and Honjo, S., 1993. *Ice-Ocean Environmental Buoys (IOEB); Technology and Deployment in 1991 – 1992,* Technical Report WHOI-93-45, Woods Hole Oceanographic Institution, 86 pp., 1993

Krishfield, R., S. Honjo, T. Takizawa, and K. Hatakeyama, *IOEB Archived Data Processing and Graphical Results from April 1992 through November 1998*, Technical Report of the Woods Hole Oceanographic Institution, WHOI-99-12, 91 pp., 1999.

Maslanik, J.A., M.C. Serreze, and T. Agnew, On the record reduction in 1998 western Arctic sea-ice cover, *Geophys. Res. Lett.*, 26, 1905-1908, 1999.

Maykut, G.A. and M.G. McPhee, Solar heating of the Arctic mixed layer, *J. Geophys. Res.*, 100, 24,691-24,703, 1995.

Maykut, G.A. and N. Untersteiner, Some results from a time-dependent thermodynamic model of sea ice, *J. Geophys. Res.*, 76, 1550-1575, 1971.

Maykut, G.A., Large-Scale Heat Exchange and Ice Production in the Central Arctic, *J. Geophys. Res.*, *87* , 7971-7984, 1982.

McPhee, M.G., The effect of the oceanic boundary layer on the mean drift of pack ice: application of a simple model, *J. Phys. Oceanogr.*, 9, 388-400, 1979.

McPhee, M.G., Turbulent heat flux in the upper ocean under sea ice, *J. Geophys. Res.*, 97, 5365-5379, 1992.

McPhee, M.G., and T.P. Stanton, Turbulence in the statically unstable oceanic boundary layer under Arctic leads, *J. Geophys. Res.*, 101, 6409-6428, 1996.

McPhee, M.G., Turbulent stress at the ice/ocean interface and bottom surface hydraulic roughness during the SHEBA drift, *J. Geophys. Res.*, 107(C10), 8037, doi:10.1029/200JC000633, 2002.

McPhee, M.G., and N. Untersteiner, Using sea ice to measure vertical heat flux in the ocean, *J. Geophys. Res.*, 87, 2071-2074, 1982.

McPhee, M.G., T.P. Stanton, J.H. Morison, D.G. Martinson, Freshening of the upper ocean in the Arctic: Is perennial sea ice disappearing? *Geophys. Res. Lett.*, *25*, 1729-1732, 1998.

Morison, J.H., S.P. Burke, H. Steltner and R. Andersen, SALARGOS temperature-conductivity buoys, *Proceedings of Oceans `82*, IEEE, 1255-1260, 1982.

Morison, J.H., J.D. Smith, Seasonal Variations in the Upper Arctic Ocean as Observed at T-3, *Geophys. Res. Lett.*, *8*, 753-756, 1981.

Moritz, R.E. et al. (eds), *SHEBA a research program on the Surface Heat Budget of the Arctic Ocean*, ARCSS/OAII Report Number 3, University of Washington, Seattle, 34 pp., 1993.

Perovich, D.K., W.B. Tucker III, and R.A. Krishfield, Oceanic heat flux in Fram Strait measured by a drifting buoy, *Geophys. Res. Lett.*, 16, 995-998, 1989.

Perovich, D.K., B.C. Elder, J.A. Richter-Menge, Observations of the annual cycle of sea ice temperature and mass balance, *Geophys. Res. Lett.*, *24*, 555-558, 1997.

Perovich, D.K., and B. Elder, Estimates of ocean heat flux at SHEBA, Geophys. Res. Lett., 29(9), doi:10.1029/2001GL014171, 2002.

Proshutinsky, A., R.H. Bourke, and F.A. McLaughlin, The role of the Beaufort Gyre in the Arctic climate variability: Seasonal to decadal climate scales, *Geophys. Res. Lett.*, 29(23), 2100, doi:10.1029/2002GL015847, 2002.

Proshutinsky, A.Y., and M.A. Johnson, Two circulation regimes of the wind-driven Arctic Ocean, *J. Geophys. Res.*, 102, 12,493-12,514, 1997.

Serreze, M.C., J.A. Maslanik, T.A. Scambos, F. Fetterer, J. Stroeve, K. Knowles, C. Fowler, S. Drobot, R.G. Barry, and T.M. Haran, A record minimum arctic sea ice extent and area in 2002, *Geophys. Res. Lett.*, 30, 1110, doi:10.1029/2002GL016406, 2003.

Steele, M., and T. Boyd, Retreat of the cold halocline layer in the Arctic Ocean, J. Geophys. Res., 102, 10,419-10,435, 1998.

Steele, M., and J.H. Morison, Hydrography and vertical fluxes of heat and salt northeast of Svalbaard in Autumn, *J. Geophys. Res.*, 98, 10,013-10,024, 1993.

Steele, M., R. Morley, and W. Ermold, PHC: A global ocean hydrography with a high-quality Arctic Ocean, *J. Climate*, 14, 2079-2087, 2001.

Walsh, J.E., W.L. Chapman, and T.L. Shy, Recent decrease of sea level pressure in the central Arctic, *J. Climate*, 9, 480-485.

Wettlaufer, J.S., Heat flux at the ice-ocean interface, *J. Geophys. Res.*, 96, 7215-7236, 1991.

Yang, J., J. Comiso, R. Krishfield, and S. Honjo, Synoptic storms and the development of the 1997 warming and freshening event in the Beaufort Sea, *Geophys. Res. Lett.*, 28, 799-802, 2001.